

UC Davis

UC Davis Previously Published Works

Title

Hierarchically nested river landform sequences. Part 1: Theory

Permalink

<https://escholarship.org/uc/item/8fk1f60b>

Authors

Pasternack, Gregory B
Baig, Dastagir
Weber, Matthew D
[et al.](#)

Publication Date

2018-05-09

DOI

10.1002/esp.4411

Data Availability

The data associated with this publication are available upon request.

Peer reviewed

1 Title: Hierarchically nested river landform sequences. Part 1: Theory

2

3 Short title: Nested river landforms sequences, part 1

4

5 Authors: Gregory B. Pasternack*, Dastagir Baig, Matthew D. Weber, Rocko A. Brown

6

7 University of California, Davis, One Shields Avenue, Davis, CA 95616, USA

8

9 * Corresponding author. Tel.: +1 (530) 302-5658

10 E-mail: gpast@ucdavis.edu

11

12 **Keywords:** river topography, river classification, flow convergence routing, fluvial
13 geomorphology

14

15 **Twitter:** River elevation and width have scale-independent, organized patterns that
16 classify to reveal the process of flow convergence routing

17

18

19 **Cite as:** Pasternack, G. B., Baig, D., Webber, M., Brown, R. 2018. Hierarchically nested
20 river landform sequences. Part 1: Theory. *Earth Surface Processes and Landforms*.

21 DOI: [10.1002/esp.4411](https://doi.org/10.1002/esp.4411).

22

23 **Abstract**

24 Past river classifications use incommensurate typologies at each spatial scale and do
25 not capture the pivotal role of topographic variability at each scale in driving the
26 morphodynamics responsible for evolving hierarchically nested fluvial landforms. This
27 study developed a new way to create geomorphic classifications using metrics
28 diagnostic of individual processes the same way at every spatial scale and spanning a
29 wide range of scales. We tested the approach on flow convergence routing, a
30 geomorphically and ecologically important process with different morphodynamic states
31 of erosion, routing, and deposition depending on the structure of nondimensional
32 topographic variability. Five nondimensional landform types with unique functionality
33 represent this process at any flow; they are nozzle, wide bar, normal channel,
34 constricted pool, and oversized. These landforms are then nested within themselves by
35 considering their longitudinal sequencing at key flows representing geomorphically
36 important stages. A data analysis framework was developed to answer questions about
37 the stage-dependent spatial structure of topographic variability. Nesting permutations
38 constrain and reveal how flow convergence routing morphodynamics functions in any
39 river the framework is applied to. The methodology may also be used with other
40 physical and biological datasets to evaluate the extent to which the patterning in that
41 data is influenced by flow convergence routing.

42

43 **Introduction**

44

45 River classification background

46

47 Geomorphic river classification serves a variety of purposes (Frissell, 1986; Brierley
48 and Fryirs, 2000; Faustini, 2012) and has a rich history reflecting different perspectives
49 on what aspects all rivers have in common and what differentiates them (Shen *et al.*,
50 1981; Rosgen 1994; Kasprak *et al.*, 2016). Many classifications are predicated on the
51 theory that geomorphic processes (i.e., dynamic mechanisms of topographic/lithologic
52 change and stability) create a characteristic assemblage of landforms (Davis, 1909;
53 Thornbury, 1954). The literature on fluvial processes cites many different geophysical
54 and chemical mechanisms governing morphodynamics (Johnsson and Meade, 1990;
55 Hancock *et al.*, 1998; Alonso *et al.*, 2002; Yumoto *et al.*, 2006; Kleinhans, 2010). Wyrick
56 and Pasternack (2015) mapped 19 different geomorphic processes occurring on a
57 single 37-km segment of a gravel/cobble bed river.

58 Unfortunately, the process-morphology linkage may be confounded by equifinality
59 (Thornbury, 1954). For example, a pool may be formed by a heterogeneous flow regime
60 (De Almeida and Rodríguez, 2012) via a diversity of mechanisms, such as turbulence-
61 induced local scour associated with a forcing element (Thompson, 2006), phase shifts
62 in the location of peak shear stress associated with one-dimensional sediment transport
63 (Wilkinson *et al.*, 2004), flow-convergence routing driven by locally varying cross-
64 sectional areas (MacWilliams *et al.*, 2006), helical hydraulics driving lateral migration
65 (Thompson, 1986), differential scour and deposition driven by differences in sediment

66 size distributions along a channel (De Almeida and Rodríguez, 2011), particle queuing
67 and selective sediment sorting (Naden and Brayshaw, 1987), and changes in the
68 relative balance of sediment supply to sediment transport capacity at the reach scale
69 (Montgomery and Buffington, 1997). As a result, inference of a river's process sets by
70 description of river morphology (and heuristic correspondence to associated processes
71 at any scale) is a challenging, open inverse problem yet commonly done (e.g., Frissell
72 et al., 1986; Rosgen, 1994; Brierley and Fryirs, 2000). Meanwhile, several reach-scale
73 river classification methods segregate by the magnitude of simple erosion potential
74 metrics (e.g., reach-scale shear stress or stream power functions), usually computed
75 from contributing catchment area, local slope, and fitted parameters (e.g., Flores *et al.*,
76 2006; Schmitt *et al.*, 2007). However, these are based on physics assumptions readily
77 violated in many rivers, even at the reach scale. In addition, erosion potential metrics
78 are incapable of accounting for and differentiating multiple processes occurring at the
79 same time and in close proximity. These considerations motivated a new approach for
80 process-linked geomorphic classification that is independent of spatial scale and thus
81 may be hierarchically nested within itself.

82

83 Classifying with a process indicator

84

85 Scientific and practical applications using river classification need more detailed and
86 more accurate representation of physical processes and how they shape landform
87 patterns. Earth's surface physical processes are driven by climatic and tectonic force
88 regimes, such as those associated with air, water, and sediment flux. Different

89 magnitudes of the driving force regime can affect a process differently. Processes are
90 also highly sensitive to the boundary conditions of the local setting.

91 In this study, we propose a conceptually new framework for process-based
92 geomorphic classification (not only for rivers) that involves four steps: (i) conceptualize
93 the suite of Earth surface physical processes governing a study domain at multiple
94 scales, (ii) identify a metric capable of representing the status of each process at any
95 location that is scale-independent for use across all magnitudes of the driving force
96 regime, (iii) create a spatially continuous analysis and classification of process metrics
97 for each mechanism at each important magnitude of the driving force regime (e.g.,
98 calm, normal, and aggressive conditions), and (iv) nest results from different levels of
99 forcing to reveal the hierarchical structure of the mechanistic assemblage. Applying this
100 generic conceptual framework to rivers involves considering a hydrological force
101 regime.

102
103 Study purpose

104
105 The overall study goal involved developing and demonstrating the new classification
106 approach theorized above by performing a continuous, multi-stage analysis of one
107 corroborated, explicit morphodynamic mechanism- flow convergence routing. The
108 classification can be applied to any river, whether alluvial or bedrock, to help interpret
109 the role of this morphodynamic mechanism. Given the breadth of this study to explain
110 new theoretical developments, test the key, underlying hypothesis against observational
111 data, and present new scientific findings using real river data, the work is divided across

112 two articles. This article presents the new landform classification theory and the
113 landform analysis concepts to be applied to classification results. Across the two articles
114 this study reveals new basic insights into process-morphology linkages in rivers and
115 demonstrates how linkages can be used in river classification in the 21st century given
116 the emergence of meter-scale digital elevation models of river networks. Now that this
117 has been done for one physical process, it can be replicated for multiple processes,
118 eventually leading to a merged classification accounting for all the processes in a river,
119 followed by a comparison among diverse rivers.

120

121 **Flow Convergence Routing Landform Classification**

122

123 Detrended bed elevation (a surrogate for depth) has been used to classify rivers
124 using the zero-crossing method (Church, 1972; Milne, 1982; Carling and Orr, 2000),
125 which yields two landforms— crest and trough. The problem with this for understanding
126 geomorphic mechanisms like flow convergence routing is that they are driven by
127 channel nonuniformity occurring as much or more in width than depth. The new
128 classification has four archetypes representing the endmember combinations of linked
129 oscillations in width and detrended bed elevation (Figure 1), with a fifth type (not shown)
130 involving a channel of average dimensions. Because the classes depend on derived
131 variables in a morphodynamic theoretical framework, it is helpful to understand the
132 scientific literature underpinning this system as well as the data and workflow for
133 obtaining the variables used to make the classification.

134

135 Flow convergence routing review

136

137 Typical erosion and deposition analysis of rivers focuses on the central tendency of
138 a river (i.e., bankfull width, bankfull depth, and reach-average slope) on the assumption
139 that the river is uniform and subjected to nearly steady flow, resulting in gradual spatial
140 and temporal trends in elevation (e.g., Gasparini *et al.*, 2004; Ferguson, 2005).

141 However, studies reporting natural channel and floodplain morphodynamics rarely
142 describe such incision and/or deposition periods consistent with the simple math of
143 central tendency of fluvial form (Kleinhans, 2010). In contrast, fluvial physical processes
144 typically exhibit abrupt and complex spatial and/or temporal variabilities (Ashworth and
145 Ferguson, 1986; Jerolmack, 2011; Wyrick and Pasternack, 2015). Meander migration,
146 knickpoint migration, braiding, pool-riffle formation and maintenance, gullying, channel
147 cut-offs, etc. involve deviations from central tendency, not specific values of central
148 tendency. In other words, having uniformly more or less erosive potential in a reach is
149 not the defining aspect of fluvial morphodynamics. Therefore, an essential step in
150 producing a mechanistic river classification must address spatial variability.

151 One important morphodynamic mechanism entirely founded on topographic
152 deviation from central tendency is called flow convergence routing (MacWilliams *et al.*,
153 2006), where flow convergence relates to the hydraulic aspect of the mechanism and
154 routing relates to its sediment dynamics. In its most general conceptualization, this
155 mechanism involves longitudinally varying spatial funneling of flow (i.e., “flow
156 convergence”) by the nonuniform topography that is inundated by the river, with the
157 locations of most concentrated flow (i.e., geometric constrictions or nozzles) at any

158 discharge having the greatest potential to scour and route sediment through them
159 (Carling and Wood, 1994; Booker *et al.*, 2001; MacWilliams *et al.*, 2006; Caamaño *et*
160 *al.*, 2009). In contrast, the locations of least concentrated flow at any discharge have
161 flow divergence and the highest likelihood of sediment deposition at that flow.
162 Secondly, rivers can have abrupt expansion zones downstream of a nozzle that can
163 sustain sediment routing and enhanced erosion caused by high turbulence intensity
164 (Clifford, 1993; Thompson *et al.*, 1996; Thompson, 2006). When a longitudinal pattern
165 of strongly convergent and divergent flow is present at any discharge, then there will be
166 spatially differentiated erosion, routing, and deposition governed by the topographic
167 structure, and this pattern will vary with discharge as controlled by the topographic
168 regime. Finally, a naturally varying hydrograph will serve as the driving force regime to
169 produce a morphodynamic time sequence of patterns of erosion, routing, and
170 deposition. As a result, flow convergence routing is a complete hydraulic and
171 morphodynamic mechanism that functions in space and time. Because it is extremely
172 difficult to observe and record spatial patterns of fluvial morphodynamics as they occur
173 in a river, flow convergence routing is most commonly detected by looking for its
174 hydraulic and topographic indicators, but the mechanism itself is a morphodynamic one,
175 not just a hydraulic pattern.

176 Because the structure of nonuniform local topography changes with discharge in
177 many settings (Brown and Pasternack, 2014, 2017), the pattern of flow funneling is
178 stage-dependent; therefore, the locations of scour and deposition shift with discharge.
179 Studies that only investigated base flow to bankfull discharge focused on the notion of a
180 two-stage “reversal” in the epicenter of scour, from riffles at low flow to pools at bankfull

181 flow (e.g., Cao *et al.*, 2003; Jackson *et al.*, 2015). Some have now considered moderate
182 to large floods that showed a diversity of flow funneling behaviors as a function of
183 discharge (Sawyer *et al.*, 2010; Strom *et al.*, 2016). Further, Brown and Pasternack
184 (2014, 2017) looked at the role of flow-dependent variability over a wide range of base
185 to flood flows in modulating channel change locally and detecting coherent patterns of
186 bed and width oscillations, respectively. Thus, to understand how morphodynamics
187 driven by flow convergence routing is governed by the combination of input flow regime
188 and topography, it is necessary to ascertain the nested structure of topographical
189 deviations from central tendency. This new research asks if patterns of topographic
190 variability can be classified based on a geomorphic process interpretation, and if so,
191 what that reveals about nested topographic patterning.

192 Flow convergence routing is but one of many fluvial processes. It has known
193 ecological importance (Wheaton *et al.*, 2010) that should be assessed in a mechanistic
194 framework. Other processes involving secondary flow hydraulics, pool bypassing over
195 point bars, bed material heterogeneity, fluctuations in turbulent intensity, sediment
196 supply regimes, etc. could also be important to characterize. They may also interact
197 with flow convergence routing.

198 This study focused on how morphodynamics (as interpreted using velocity as an
199 indicator of flow convergence routing) are driven by nonuniform topographic structure,
200 but morphodynamics in turn change topographic structure as well. Therefore, there is
201 some duality in analysis. On one hand, the present structure provides insights into what
202 must have happened to get to the current state, and on the other hand, it indicates what
203 comes next. For example, a geological nozzle (Kieffer, 1989) could either exist because

204 it is composed of a highly resistant lithology that cannot erode or from a pause in
205 transient morphodynamics of equally erodible material that left that spot constricted.
206 Either way, flow convergence routing dictates that it will be the epicenter of erosive
207 potential during the next nozzle activation event. Whether one wants to understand the
208 past, the future, or just transient morphodynamics in and of itself, an analysis of
209 topographic structure deviating from central tendency as related to flow convergence
210 routing ought to be meaningful, and that is what this study aims to evaluate.

211

212 Data processing workflow

213

214 A standardized, universal workflow yields the variables for the new classification
215 (Figure 2). The entire workflow is achievable with a single data input– a high-resolution
216 (~ 1-m) digital elevation model (DEM) of a river valley (Gore and Pasternack, 2016),
217 making this methodology readily accessible. However, improved results are achieved
218 given geomorphic reach breaks obtained from expert evaluation and water surface area
219 polygons for selected discharges obtained from two-dimensional (2D) hydrodynamic
220 modeling. Velocity results from 2D modeling can confirm the velocity hypotheses built
221 into flow convergence routing classification for confidence in the mechanistic
222 interpretation.

223 Workflow steps are conceptually straightforward, but require many minor decisions
224 depending on data nuances for any given river. The overall strategy involves extracting
225 longitudinal series of bed elevation and top width, and then analyzing their joint
226 geometric structure (Brown and Pasternack, 2014, 2017). This section presents the

227 recommended approach for each step, but also discusses uncertain complexities
228 involved in geometric analysis of river corridors.

229 Traditionally, geomorphic longitudinal analysis follows the thalweg and analyzes
230 thalweg bed elevation, but in this workflow the bisecting centerline of the water surface
231 area is superior for two reasons. First, because some channels can be highly sinuous
232 and/or thalweg sinuosity may not align with bank sinuosity, cross sections stationed
233 along the thalweg can overlap or even double back into the channel upstream or
234 downstream. Second, thalweg depth is the maximum possible water depth for a cross
235 section (Figure 3), and thus it significantly overestimates cross-sectional area. Given a
236 complete river corridor DEM, one can directly calculate cross-sectionally averaged
237 depth, and this is the correct variable to compute a cross-sectional area. The
238 convention of using top width is retained in this workflow.

239 Although many geomorphologists seek DEM-only analysis methods (Drăguț and
240 Eisank, 2011; Wheaton *et al.*, 2015), a lack of hydraulic information complicates
241 mapping inundated area to extract top width longitudinal series. It is possible to slope
242 detrend a DEM and take horizontal water surface slices through and above the
243 detrended terrain (e.g., Jones, 2006; Greco *et al.*, 2008), thereby transforming ground
244 elevation into a measure of water depth for each slice, which then enables a
245 determination of stage-dependent width. However, the corresponding discharge of each
246 slice is uncertain.

247 Many methods of slope detrending exist, but there are significant problems with all
248 detrending methods— a topic that is beyond the scope of this study. It is accessible to
249 use the slicing approach with any preferred slope-detrending method. Performing

250 coarse-resolution hydraulic simulations is easy, fast, and more accurate than slope
251 detrending. From one perspective, modeling is a methodology for slope detrending, just
252 one based on the laws of physics rather than unconstrained geometric modeling. High-
253 resolution 2D hydrodynamic modeling provides the most detailed water surface area
254 polygons.

255 The framework developed in this study assesses the relative cross-sectional area
256 along the flow path. Given the bisecting centerline of the water surface area at each
257 flow, the stationing interval is user-selectable, informed by DEM resolution and channel
258 size. We recommend a spacing of ~ 3-5% of bankfull width. Mean bed elevation is
259 computed in a rectangle centered on each centerline station and clipped by the water
260 surface area boundary for each flow (See Figure 4 of Wyrick and Pasternack (2014) for
261 a map illustration of such rectangles). This value was assigned to the centerline station
262 point in the rectangle. The longitudinal profile of mean bed elevation is detrended on a
263 piecewise linear basis, with each geomorphic reach detrended independently. The
264 slope trend equation for each reach is determined using linear regression. Next, the
265 mean and standard deviation of detrended bed elevation is computed for the entire river
266 segment. These values are used to standardize the variable by subtracting the mean
267 and dividing by the standard deviation. The resulting series of detrended, standardized,
268 cross-sectionally averaged bed elevation (Z_s) is a nondimensional surrogate for
269 average water depth useful for comparing relative magnitude along the profile; however,
270 bed elevation has the opposite interpretation as depth (i.e., high Z_s equals low depth,
271 Figure 1).

272 Width at each centerline station is computed as the water surface area of the clipped
273 rectangle for that station divided by the user-selected length of the rectangle. This
274 method is superior to cross-section line width for flow convergence routing assessment,
275 because it averages along a length to give a more representative value. Mean and
276 standard deviation of width are computed for the entire river segment. These values are
277 used to standardize the variable by subtracting the mean and dividing by the standard
278 deviation. The resulting series of standardized width (W_s) is a nondimensional hydraulic
279 variable useful for comparing relative magnitude along the profile.

280 Width is explicitly a hydraulic variable, so it does not necessarily require detrending
281 the way bed elevation does to understand its influence on flow convergence routing. If
282 discharge is constant along a study reach, then any systematic change in width along
283 the reach influences the morphodynamic mechanism and should be used in the
284 classification. If major tributaries bring additional water into a reach, then it may be
285 necessary to evaluate whether detrending to remove that hydrological effect would be
286 warranted prior to classification.

287

288 Classification decision tree

289

290 A consideration of the signs and magnitudes of W_s and Z_s reveal a simple 5-unit
291 classification of geometry (Figures 1-2). Four geometric possibilities depend primarily on
292 the combination of signs of W_s and Z_s (Brown and Pasternack, 2017). The fifth
293 landform type recognizes that there must be a baseline, normal configuration indicated

294 by W_s and Z_s value close to zero. A decision tree was developed to classify each
295 centerline station at each flow using two-character identification codes (Figure 2).

296 The question is how strongly must geometry deviate from the average to be
297 considered significant enough to denote a new landform type as a starting point before
298 many data sets can be analyzed for possible threshold criteria? We have piloted this
299 methodology using three river datasets, one from a gravel/cobble river (see Pasternack
300 et al., 2018) and two from mountain bedrock-boulder rivers (Gore and Pasternack,
301 2016). Using those datasets, sensitivity analysis was done to answer this, but these
302 details are too lengthy to cover herein. Conceptually, the more that $W_s \cdot Z_s$ threshold
303 values deviate from zero, the more uniform a river will seem. Depending on the
304 application, a geomorphologist may wish to choose lower or higher threshold values at
305 their discretion. The $W_s \cdot Z_s$ threshold values we recommend and used in Pasternack et
306 al. (2018) were -0.5 and 0.5, yielding a wide range in $W_s \cdot Z_s$ for the baseline, “normal
307 channel” landform type. These numbers are conservative, equidistance thresholds in
308 the sense of assuming much more of the river is normal, not only because of the wide
309 range of $W_s \cdot Z_s$ values, but also because it does not constrain the individual W_s and Z_s
310 values. For example, using the base flow gravel/cobble bed lower Yuba River data from
311 Pasternack et al. (2018) as an example, ~ 60% of stations with $-0.5 < W_s \cdot Z_s < 0.5$ had
312 individual W_s and Z_s values also meeting that same criterion.

313 Note that it is possible to conceive of many alternate ways to set flow convergence
314 routing landform classification criteria. A similar but more exacting and specific system
315 requires both variables to individually exceed a threshold (Figure 4a). A more
316 comprehensive system adds in four more classes to account for when one variable

317 strongly deviates but the other does not (Figure 4b). The mechanistic validity of the
318 approach selected for this study was tested in Pasternack et al. (2018). Using the
319 product $Ws \cdot Zs$ and the thresholds of -0.5 and 0.5, flow convergence routing was
320 confirmed, so this worked. Whether the proposed alternative classifications would work
321 better has not yet been tested.

322

323 **Landform Analysis Concepts**

324

325 The classification described in the previous section is not an end unto itself, but a
326 means for evaluating the patterning of a river's topography with respect to flow
327 convergence routing. Many methods analyze the longitudinal sequencing of landforms
328 (e.g., Richards, 1976; Grant et al. 1990). Wyrick and Pasternack (2014) introduced an
329 object-oriented framework for two-dimensional spatial analysis of landforms addressing
330 abundance, diversity, adjacency, lateral variability, and longitudinal distribution and
331 spacing. Legleiter (2014) introduced a geostatistical framework for analyzing river DEMs
332 and began the effort of linking resultant new metrics to morphological features. Brown
333 and Pasternack (2017) applied spectral and statistical methods to analyze high-
334 resolution width and detrended bed elevation series. Past methods can be used directly
335 or adapted for analysis of the spatial structure of flow convergence routing landforms.
336 The key nuance is that these landforms are explicitly indicative of a morphodynamic
337 mechanism, so there is a unique potential for analysis to explain how flow and
338 topography interact to produce these landforms and drive future morphodynamics.

339 There are three broad categories of data analysis envisioned to understand the
340 results of the classification with no other data inputs. A fourth category of analysis
341 involves testing for the underlying hydraulic mechanism involved in flow convergence
342 routing using velocity data. Once the topographic structure of the river is understood
343 with these analyses, then the classification objects may be used with other datasets the
344 evaluate the nexus between flow convergence routing and patterns in the other data.

345

346 Analysis of W_s , Z_s , and $W_s \cdot Z_s$ series

347

348 The first step of landform analysis involves steps similar to those of Brown and
349 Pasternack (2017), which is to first understand the stage-dependent structure of fluvial
350 topographic deviation from central tendency using the W_s and Z_s series. As a
351 community, we do not know the scope and organization of global W_s and Z_s variability.
352 The degree to which W_s and Z_s deviate from their central tendencies can be quantified
353 by simple tabulation of the percent of Z_s and W_s values more than one-half, one, or
354 more standard deviations away from the mean, depending on the application. Besides
355 knowing the frequency of variability, it is also important to ascertain its randomness. The
356 non-parametric test for the number of runs of Z_s or W_s values above and below the
357 median determines whether a series is random or not (Wald and Wolfowitz, 1940). To
358 see if W_s and Z_s are linked as implied by the flow convergence routing mechanism,
359 Pearson's product-moment correlation analysis can be used to compare the two series,
360 and this should be done by reach and for each flow. Finally, for flow convergence
361 routing to be important at a given spatial scale for a reach as a whole, the mean and

362 median of the product $W_s \cdot Z_s$ should be above zero (Brown and Pasternack, 2017).
363 Analysis of the $W_s \cdot Z_s$ series reveals where this is occurring or not, and this varies by
364 discharge. For example, in a boulder-dominated mountain river one would expect the
365 median of $W_s \cdot Z_s$ to be negative from base flow to possibly quite a high flood flow.
366 Eventually, when the flow is reached that is powerful enough to re-organize the boulder
367 framework, then the median of $W_s \cdot Z_s$ would be positive, and this switch would be
368 diagnostic of the onset of the flood flow range that is morphodynamically significance.

369

370 Analysis of landform abundance and sequencing

371

372 Analysis of landforms abundance and sequencing evaluates the presence of
373 organizational tendencies and their implications for morphodynamics. For flow
374 convergence routing to be a dominant morphodynamic process controlling the landform
375 patterning in a river, there must be a range of discharges for which wide bar and
376 constricted pool are more abundant than oversized and nozzle. Further, the sequencing
377 of landforms should alternate between wide bar and constricted pool, which would
378 necessitate some length of normal channel in between to make the transition.

379 Abundance of each landform class is determined by counting the number of stations
380 of each landform type and computing relative percent. Some landforms are thought to
381 co-occur, but this is rarely tested (e.g., Grant *et al.*, 1990; Wyrick and Pasternack,
382 2014). In the analysis framework for this study, the number of times that each unit type
383 follows each other can be computed. This test should be performed first using all
384 landform types, but then a second time without normal channel. This second step is

385 necessary because it is mathematically impossible to transition directly from a landform
386 type with $-W_s \cdot Z_s$ to one with $+W_s \cdot Z_s$ without going through $W_s \cdot Z_s = 0$. It may be that the
387 length of the normal channel units is small in these transitions, so excluding them
388 provides a way to quantify the tendencies for how the other units are sequenced. These
389 abundance and sequencing analyses should be performed for a whole river corridor and
390 individual reaches, and that is repeated for each flow investigated.

391

392 Analyses of hierarchical landform nesting

393

394 The most novel and important analyses developed in this study reveal and assess
395 nested landforms structure. Bankfull flow is widely thought responsible for shaping
396 channel landforms. However, this implies specific landform nesting permutations. For
397 example, under conventional theory, a bankfull nozzle should promote scour of the
398 things inside of it. If a depositional wide bar was nested in a bankfull nozzle, then that
399 would contradict the classic expectation. If the inset bed material was substantially finer,
400 then it would indicate a role for lower flows depositing potentially ephemeral inset
401 landforms (e.g., benches) likely on a rapidly falling limb of a flood. On the other hand, if
402 bed material is the same for bankfull and nested smaller landforms, then it would
403 strongly suggest that bankfull and baseflow nested landforms were emplaced at the
404 same time as a result of a significantly larger flow.

405 A decision has to be made how many discharges to use for nesting analysis.

406 Although landforms sequences could be analyzed in each of many flows across the
407 discharge continuum, it is likely that there would be a lot of insignificant correlation in

408 such an incremental approach. Therefore, the valley-scale patterning of the river
409 corridor can inform the meaningful flows to analyze. For a simple channel-floodplain
410 pairing in a wide valley floor with low slope and fine sediment, two discharges may be
411 sufficient- baseflow and bankfull flow. If there exists a macrochannel tiered structure
412 (e.g., Croke *et al.*, 2014), then one discharge per terrace level would be sensible. Given
413 five nested terraces combining to steer morphodynamics, there would be 3125
414 permutations of nested landforms- a scope of river classification never before
415 considered, and this is for just one fluvial mechanism. Of course, many theoretical
416 permutations may prove nonexistent in nature– in Pasternack et al. (2018) 1/3 were
417 nonexistent. Still, a very simple mechanistic conceptualization can produce an
418 extraordinarily complex and complete understanding of how a single process is
419 functioning across scales.

420 Most commonly, three discharges are likely to be most useful, consisting of
421 baseflow, bankfull flow, and a representative flood flow constrained by proximal valley
422 hillsides. One sensible choice would be the flow filling the floodprone area (Rosgen
423 (1994). Given five landform types and three nested scales, there are 125 possible
424 landform permutations- again, several of these may be nonexistent.

425 The recommended workflow for analysis of landform nesting once the number of
426 flows is decided involves joining the landform ID series for all flows to a common
427 centerline and analyzing the structure hierarchical permutations. Because the length of
428 a sinuous river centerline often decreases with discharge, the centerline stationing of
429 the lowest flow is the best choice for this analysis (Brown and Pasternack, 2017). The
430 primary analysis of nested data involves counting the frequency of each permutation to

431 ascertain the top 3-5 most frequently occurring nesting permutations. Beyond just
432 overall permutations across all three scales and five landform types, it is informative to
433 consider the top permutations by landform, because this extra analysis is independent
434 of the relative abundance of landforms. This extra analysis can be done by starting with
435 a given flood discharge landform type and seeing what is nested within that. The same
436 can be done for looking at bankfull landforms and seeing both what these are nested
437 within at a higher flow and what is nested within them at a lower flow. Results can be
438 compared to those expected in an ideal scenario with flow convergence routing.

439

440 Validating the hydraulic mechanism

441

442 The classification presented herein is predicated on the past literature showing that
443 wide, shallow riffles and deep, narrow pools exhibit specific stage-dependent
444 differences in velocity (V) associated with flow convergence routing (Sawyer *et al.*,
445 2010; Strom *et al.*, 2016). Even if highly conservative criteria delineate normal channel
446 geometry, it is always wise to test whether the fundamental hydraulic hypothesis
447 underlying the mechanism of flow convergence routing holds with this classification that
448 assumes it does. There are three reasons why the classification might not yield the
449 anticipated hydrogeomorphic mechanism. First, the magnitude of width and depth
450 constriction or expansion might not be extreme enough to trigger a significant enough
451 deviation in velocity to cause flow convergence routing. If that was the case, then the
452 decision tree classification could be revised and the outcome re-tested. Second, there
453 might be strong enough geometric deviations, but the resulting 2D velocity field could

454 exhibit a much different effective flow width (i.e., the fraction of width carrying the
455 majority of flow as in Harrison and Keller, 2007), yielding a different mechanism than if
456 the entire cross section was active. For example, an oversized landform would be
457 expected to have low velocity, but if the effective flow width was 1/10 of the full width,
458 then it would have a much higher peak velocity than average velocity. Third, it is
459 possible that the differentiation in velocity between landforms is not due to differences in
460 cross-sectional area, but differences in bed roughness and/or slope. Therefore, testing
461 with 2D velocity rasters can reveal if the classification is actually capturing flow
462 convergence routing or not.

463 To do a velocity validation analysis of the classification, 2D numerical modeling
464 (Pasternack, 2011) is needed, because the mechanistic deviations from expectation
465 cannot be adequately revealed by analytical, empirical, or one-dimensional numerical
466 velocity estimation methods. Given a 2D model, velocity rasters for discharges ranging
467 from baseflow to as high of a flood flow as possible should be obtained. These rasters
468 are then stratified by landform type. Finally, the landform-averaged velocity and 95th
469 percentile of velocity of raster cells in that landform are computed (e.g, Strom *et al.*,
470 2016).

471 For this classification to adhere to theory, oversized should have a low velocity,
472 nozzle should have a high velocity, and normal channel should have an intermediate
473 velocity between those two. These relative magnitudes should hold across all
474 discharges. Meanwhile, constricted pool and wide bar should have flow-dependent
475 relative velocities, with the former having a higher velocity than both normal channel
476 and wide bar during floods. How wide bar versus oversized velocity might compare as

477 well as how constricted pool versus nozzle velocity, is an open question investigated in
478 Pasternack et al. (2018), given the possibility of a narrower effective flow width in one or
479 more landform types.

480

481 **Discussion**

482

483 Geomorphologists have long believed that rivers have a diversity of organized
484 landforms, yet still many quantitative analyses of process-morphology linkages assume
485 uniform flow. While rivers in general exhibit a central tendency of increasing erosive
486 potential with discharge, evidence from several individual sites firmly establishes that
487 rivers do not have to work that way, because hierarchical scales of longitudinally
488 organized topographic complexity yield a different mechanism than widely assumed
489 based on the uniform flow assumption used throughout geomorphology. The
490 overwhelming evidence of nonuniform flow creates an imperative to the progression of
491 the discipline that geomorphologists abandon the math of uniform flow for everything
492 from river classification and assessment to landscape evolution modeling in favor of
493 methods that account for topographic variability as well as the resulting spatial hydraulic
494 variability. In addition to multidimensional numerical modeling tools, this study offers a
495 topographical analysis workflow that allows practitioners to classify and analyze fluvial
496 topographic complexity to interpret a river corridor's potential for one important
497 mechanism, flow convergence routing.

498 This study is not about trying to find simple approaches that end the rise of 2D
499 modeling as a powerful tool for river science and engineering, but instead to provide

500 practitioners with the right tool at the right stage of activity. Studies using meter-scale
501 2D modeling over tens of kilometers of rivers are well established and showing
502 tremendous capability to reveal spatially explicit hydraulics and associated processes
503 (Pasternack, 2011). Soon scalable, parallel-processing algorithms (e.g., TUFLOW GPU
504 and JFLOW) will run meter-scale 2D simulations of entire dendritic river networks, with
505 results handed off to algorithms that will reveal hydrogeomorphic processes and
506 ecological functions. That future is very bright. Yet what is also apparent is that humans
507 still need simplified representations and abstractions to make sense of ever growing,
508 vast informatics datasets. Whether it is in lieu of cutting edge numerical modeling or to
509 synthesize modeling results, the procedures in this study quickly yield useful results that
510 practitioners can employ to assess how functional rivers are and to aid the design of
511 more functional river corridors.

512
513 Applications with other datasets

514
515 Beyond using the concepts and methods presented here to better understand
516 hierarchically nested river landforms, there is significant utility in using maps of these
517 landform polygons to assess whether a variety of hydraulic, sedimentary, geomorphic,
518 and ecological processes have a nexus with flow convergence routing. An obvious
519 application to further understand morphodynamics would be the analysis of DEM
520 difference rasters by hierarchically nested river landforms. There are specific
521 hypotheses as to what DEM differences should be necessary to create individuals of
522 each landform type as well as what DEM differences should be driven next given a

523 particular nesting and sequencing of these landforms. Another issue that has been
524 neglected in the development of this method is the important role of variations in grain
525 size for morphodynamics (Bayat *et al.*, 2017). Given bed material facies data, one could
526 evaluate the relative roles of topographic versus substrate variability. Beyond
527 geomorphology, one could look at emerging ecogemorphic topics, such as large wood
528 storage patterns in a river network relative to patterns of topographic variability. One
529 can also look at the abundance and distribution of organisms by landform type.

530 For any geospatial dataset, one may run simple tests to determine if the data is
531 present in any of the landforms more than would be expected by random chance given
532 the abundance of each landform found in a particular river. For example, if the relative
533 area of wide bar to nozzle was ten to one, but the abundance of an organism in those
534 was two to one, respectively, then that would show a significant preference for nozzle,
535 even though more are found in wide bar, because the relative abundance of nozzle is
536 so much less. It shows that the organism is packing much more densely into nozzle.

537 This concept of analyzing abundance data on an area-free basis is widespread in
538 science. In geomorphology, Grant *et al.* (1990) and Wyrick and Pasternack (2014) used
539 this concept to compare landform abundances relative to random uniform distributions.
540 Strom *et al.*, (2016) used the idea to analyze the abundance of patches of peak velocity
541 among landforms on an area-free basis.

542 In ecology, the concept is widely used, and one of the dominant area-free metrics is
543 called the forage ratio that indicates an organism's preference or avoidance for a certain
544 type of prey (Savage, 1931; Ivlev, 1961). Today, the forage ratio and other similar
545 indices are used to compare all kinds of data against other kinds of data. For example,

546 one can look at the abundance of an organism or an indicator of an ecological process
547 relative to the abundance of microhabitats of different quality or wholesale fluvial
548 landforms (Pasternack *et al.*, 2014). Kammel *et al.* (2016) developed and applied a
549 statistical bootstrapping method that quantifies the statistical significance of ratios of
550 data abundances relative to the areas of each classifying object.

551

552 **Conclusions**

553

554 This study developed new theory and methods that show how the same scale-
555 independent landform types may be mapped at many scales and nested to obtain a
556 hierarchical framework. Past morphological unit classification methods either have
557 diverse morphologies yet are fundamentally descriptive or have supposedly process-
558 based metric thresholds yet only account for the central tendency of river form that
559 actually has little to do with the direct mechanisms that cause fluvial landform patterning
560 in rivers. This study is the first fluvial classification whose landforms are explicitly
561 governed by a morphodynamic mechanism. At the highest level, this study shows that
562 it is feasible to take an individual geomorphic process, conceptualize how it operates
563 relative to hierarchical topographic complexity, produce a metric for it, and then map the
564 spatial pattern of where it does the different functions it performs over a wide range of
565 flows. Although there are many minor nuances in the methods to be debated and
566 refined as the approach is tested in different settings, the underlying concept stands up
567 to validation against more sophisticated 2D hydrodynamic modeling. It is highly feasible
568 for geomorphologists to move beyond the simple erosion potential metric that assumes

569 steady uniform flow and repeat this effort for a diversity of actual hydrogeomorphic
570 mechanism in rivers, which largely require spatio-temporal complexity, not simplicity.

571

572 **Acknowledgements**

573

574 Precursor data were collected for different purposes with funding from the Yuba
575 County Water Agency (Award #201016094) and as in-kind aid from the Yuba Accord
576 River Management Team. Time spent processing and analyzing data was funded by
577 Yuba County Water Agency (Award #201016094). This project was also supported by
578 the USDA National Institute of Food and Agriculture, Hatch project number #CA-D-
579 LAW-7034-H. We thank Dr. Roser Casas-Mulet, Joni Gore, Belize Lane, Dr. Michael
580 Stewardson, Anne Senter, and Jason Wiener for constructive reviews of a draft of this
581 manuscript prior to journal submission as well as Dr. Stuart Lane and anonymous
582 reviewers for constructive guidance in manuscript revision.

583

584 **References**

585

586 Alonso CV, Bennett SJ, Stein OR. 2002. Predicting head cut erosion and migration in
587 concentrated flows typical of upland areas. *Water Resources Research* **38**: 1303-
588 1318.

589 Ashworth PJ, Ferguson RI. 1986. Interrelationships of Channel Processes, Changes
590 and Sediments in a Proglacial Braided River. *Geografiska Annaler. Series A,*
591 *Physical Geography* **68**: 361-371. DOI: 10.2307/521527.

592 Bayat E, Rodríguez JF, Saco PM, de Almeida GAM, Vahidi E, García MH. 2017. A tale
593 of two riffles: Using multidimensional, multifractional, time-varying sediment
594 transport to assess self-maintenance in pool-riffle sequences. *Water Resources*
595 *Research* **53**: 2095-2113. DOI: 10.1002/2016WR019464

596 Booker DJ, Sear DA, Payne AJ. 2001. Modelling three-dimensional flow structures and
597 patterns of boundary shear stress in a natural pool-riffle sequence. *Earth Surface*
598 *Processes and Landforms* **26**: 553-576.

599 Brierley GJ, Fryirs K. 2000. River styles, a geomorphic approach to catchment
600 characterization: Implications for river rehabilitation in Bega catchment, New
601 South Wales, Australia. *Environmental Management* **25**: 661-679.

602 Brown RA, Pasternack GB. 2014. Hydrologic and topographic variability modulate
603 channel change in mountain rivers. *Journal of Hydrology* **510**: 551-564. DOI:
604 10.1016/j.jhydrol.2013.12.048.

605 Brown RA, Pasternack GB. 2017. Bed and width oscillations form coherent patterns in a
606 partially confined, regulated gravel–cobble-bedded river adjusting to
607 anthropogenic disturbances. *Earth Surf. Dynam.* **5**: 1-20. DOI: 10.5194/esurf-5-1-
608 2017.

609 Cao ZX, Carling P, Oakey R. 2003. Flow reversal over a natural pool-riffle sequence: A
610 computational study. *Earth Surface Processes and Landforms* **28**: 689-705.

611 Caamaño D, Goodwin P, Buffington JM, Liou JCP, Daley-Laursen S. 2009. Unifying
612 Criterion for the Velocity Reversal Hypothesis in Gravel-Bed Rivers. *Journal of*
613 *Hydraulic Engineering* **135**: 66-70.

614 Carling PA, Wood N. 1994. Simulation of flow over pool-riffle topography: A
615 consideration of the velocity reversal hypothesis, *Earth Surface Processes and*
616 *Landforms* **19**: 319-332.

617 Carling PA, Orr HG. 2000. Morphology of riffle-pool sequences in the River Severn,
618 England. *Earth Surface Processes and Landforms* **25**: 369-384.

619 Church MA. 1972. Baffin Island sandar: a study of Arctic fluvial processes. *Geological*
620 *Survey of Canada Bulletin* **216**: 1-208.

621 Clifford NJ. 1993. Formation of riffle-pool sequences: Field evidence for an autogenetic
622 process, *Sedimentary Geology* **85**: 39-51.

623 Croke J, Reinfelds I, Thompson C, Roper E. 2014. Macrochannels and their
624 significance for flood-risk minimisation: examples from southeast Queensland
625 and New South Wales, Australia. *Stochastic Environmental Research and Risk*
626 *Assessment* **28**: 99-112. DOI: 10.1007/s00477-013-0722-1.

627 Davis WM. 1909. The Geographical Cycle, Chapter 13. In *Geographical Essays*. Ginn
628 and Co.: New York.

629 De Almeida GAM, Rodríguez JF. 2011. Understanding pool-riffle dynamics through
630 continuous morphological simulations. *Water Resources Research* **47**: W01502.
631 DOI: 10.1029/2010WR009170.

632 De Almeida GAM, Rodríguez JF. 2012. Spontaneous formation and degradation of
633 pool-riffle morphology and sediment sorting using a simple fractional transport
634 model. *Geophysical Research Letters* **39**. DOI: 10.1029/2012GL051059.

635 Drăguț L, Eisank C. 2011. Object representations at multiple scales from digital
636 elevation models. *Geomorphology* **129**: 183-189. DOI:
637 <http://dx.doi.org/10.1016/j.geomorph.2011.03.003>.

638 Faustini J. 2012. *River Classification: An Overview*. A White Paper Submitted to the
639 Southeast Aquatics Resource Partnership. United States Fish and Wildlife
640 Service, Region 4. Atlanta, Georgia.

641 Ferguson RI. 2005. Estimating critical stream power for bedload transport calculations
642 in gravel-bed rivers. *Geomorphology* **70**: 33-41. DOI:
643 <http://dx.doi.org/10.1016/j.geomorph.2005.03.009>.

644 Flores AN, Bledsoe BP, Cuhaciyan CO, Wohl EE. 2006. Channel-reach morphology
645 dependence on energy, scale, and hydroclimatic processes with implications for
646 prediction using geospatial data. *Water Resources Research* **42**: W06412. DOI:
647 [10.1029/2005WR004226](http://dx.doi.org/10.1029/2005WR004226).

648 Frissell CA, Liss WJ, Warren CE, Hurley MD. 1986. A hierarchical framework for stream
649 habitat classification: Viewing streams in a watershed context. *Environmental*
650 *Management* **10**: 199-214. DOI: [10.1007/bf01867358](http://dx.doi.org/10.1007/bf01867358).

651 Gasparini NM, Tucker GE, Bras RL. 2004. Network-scale dynamics of grain-size
652 sorting: implications for downstream fining, stream-profile concavity, and
653 drainage basin morphology. *Earth Surface Processes and Landforms* **29**: 401-
654 421. DOI: [10.1002/esp.1031](http://dx.doi.org/10.1002/esp.1031).

655 Gore J, Pasternack GB. 2016. Analysis and classification of topographic flow steering
656 and inferred geomorphic processes as a function of discharge in a mountain

657 river. Abstract EP53D-1016 presented at 2016 Fall Meeting, AGU, San
658 Francisco, Calif., 12-16 Dec.

659 Grant GE, Swanson FJ, Wolman MG. 1990. Pattern and Origin of Stepped-Bed
660 Morphology in High-Gradient Streams, Western Cascades, Oregon. Geological
661 Society of America Bulletin **102**: 340-352.

662 Greco SE, Girvetz EH, Larsen EW, Mann JP, Tuil JL, Lowney C. 2008. Relative
663 Elevation Topographic Surface Modelling of a Large Alluvial River Floodplain and
664 Applications for the Study and Management of Riparian Landscapes. Landscape
665 Research **33**: 461-486. DOI: 10.1080/01426390801949149.

666 Hancock GS, Anderson RS, Whipple KX. 1998. Beyond Power: Bedrock River Incision
667 Process and Form. In *Rivers Over Rock: Fluvial Processes in Bedrock Channels*,
668 Tinkler KJ, Wohl EE (eds). American Geophysical Union; 35-60. DOI:
669 10.1029/GM107p0035.

670 Harrison LR, Keller EA. 2007. Modeling forced pool–riffle hydraulics in a boulder-bed
671 stream, southern California. *Geomorphology* **83**: 232-248. DOI:
672 <http://dx.doi.org/10.1016/j.geomorph.2006.02.024>.

673 Ivlev VS. 1961. *Experimental ecology of the feeding of fishes*. Yale University Press:
674 New Haven.

675 Jackson JR, Pasternack GB, Wheaton JM. 2015. Virtual manipulation of topography to
676 test potential pool–riffle maintenance mechanisms. *Geomorphology* **228**: 617-
677 627. DOI: 10.1016/j.geomorph.2014.10.016.

678 Jerolmack DJ. 2011. Causes and effects of noise in landscape dynamics. *Eos*,
679 *Transactions American Geophysical Union* **92**: 385-386. DOI:
680 10.1029/2011EO440001

681 Johnsson MJ, Meade RH. 1990. Chemical weathering of fluvial sediments during
682 alluvial storage; the Macuapanim Island point bar, Solimoes River, Brazil. *Journal*
683 *of Sedimentary Research* **60**: 827-842.

684 Jones JL. 2006. Side channel mapping and fish habitat suitability analysis using LIDAR
685 topography and orthophotography. *Photogrammetric Engineering and Remote*
686 *Sensing* **71**: 1202-1206.

687 Kammel LE, Pasternack GB, Massa DA, Bratovich PM. 2016. Near-census
688 ecohydraulics bioverification of *Oncorhynchus mykiss* spawning microhabitat
689 preferences. *Journal of Ecohydraulics* **1**. DOI: 10.1080/24705357.2016.1237264

690 Kasprak A, Hough-Snee N, Beechie T, Bouwes N, Brierley G, Camp R, Fryirs K, Imaki
691 H, Jensen M, O'Brien G, Rosgen D, Wheaton J. 2016. The Blurred Line between
692 Form and Process: A Comparison of Stream Channel Classification Frameworks.
693 *PLOS ONE* **11**: e0150293. DOI: 10.1371/journal.pone.0150293.

694 Kieffer SW. 1989. Geologic Nozzles. *Reviews of Geophysics* **27**: 3-38

695 Kleinhans MG. 2010. Sorting out river channel patterns. *Progress in Physical*
696 *Geography* **34**: 287-326. DOI: doi:10.1177/0309133310365300.

697 Legleiter CJ. 2014. A geostatistical framework for quantifying the reach-scale
698 morphology: 1. Variogram models, related metrics, spatial structure of river and
699 relation to channel form. *Geomorphology* **205**: 65-84.

700 MacWilliams ML, Jr., Wheaton JM, Pasternack GB, Street RL, Kitanidis PK. 2006. Flow
701 convergence routing hypothesis for pool-riffle maintenance in alluvial rivers.
702 Water Resources Research **42**. DOI: 10.1029/2005WR004391.

703 Milne JA. 1982. Bed-material size and the riffle-pool sequence. *Sedimentology* **29**, 267–
704 278.

705 Montgomery DR, Buffington JM. 1997. Channel-reach morphology in mountain drainage
706 basins. *Geological Society of America Bulletin* **109**: 596-611.

707 Naden PS, Brayshaw AC. 1987. Small and medium-scale bedforms in gravel-bed rivers.
708 In *River Channels: Environment and Process*, Richards K (ed). Basil Blackwell:
709 Oxford; 249–271.

710 Pasternack GB. 2011. *2D Modeling and Ecohydraulic Analysis*. Createspace, Seattle,
711 WA.

712 Pasternack GB, Tu D, Wyrick JR. 2014. Chinook adult spawning physical habitat of the
713 lower Yuba River. Prepared for the Yuba Accord River Management Team.
714 University of California: Davis, CA.

715 Pasternack GB, Baig D, Webber M, Brown, R. 2018. Hierarchically nested river
716 landform sequences. Part 2: Bankfull channel morphodynamics governed by
717 valley nesting structure. *Earth Surface Processes and Landforms*.

718 Richards KS. 1976. Morphology of Riffle-Pool Sequences. *Earth Surface Processes and*
719 *Landforms* **1**: 71-88.

720 Rosgen DL. 1994. A Classification of Natural Rivers. *Catena* **22**: 169-199.

721 Savage RE. 1931. The relation between the feeding of the herring off the east coast of
722 England and the plankton of the surrounding waters. London (UK): Fishery

723 Investigations, Ministry of Agriculture, Food, and Fisheries. Series II. Vol. **12**: 1-
724 88.

725 Sawyer AM, Pasternack GB, Moir HJ, Fulton AA. 2010. Riffle-pool maintenance and
726 flow convergence routing observed on a large gravel-bed river. *Geomorphology*
727 **114**: 143-160. DOI: 10.1016/j.geomorph.2009.06.021.

728 Schmitt L, Maire G, Nobelis P, Humbert J. 2007. Quantitative morphodynamic typology
729 of rivers: a methodological study based on the French Upper Rhine basin. *Earth*
730 *Surface Processes and Landforms* **32**: 1726-1746. DOI: 10.1002/esp.1596.

731 Shen HW, Schumm SA, Nelson JD, Doehring DO, Skinner MM. 1981. Methods for
732 Assessment of Stream- Related Hazards to Highways and Bridges. FHWA-RD-
733 80-160. Federal Highway Administration: Washington, DC.

734 Strom MA, Pasternack GB, Wyrick JR. 2016. Reenvisioning velocity reversal as a
735 diversity of hydraulic patch behaviours. *Hydrological Processes* **30**: 2348-2365.
736 DOI: 10.1002/hyp.10797.

737 Thompson A. 1986. Secondary flows and the pool-riffle unit: A case study of the
738 processes of meander development. *Earth Surface Processes and Landforms*
739 **11**: 631-641. DOI: 10.1002/esp.3290110606.

740 Thompson DM, Wohl EE, Jarrett RD. 1996. A revised velocity reversal and sediment
741 sorting model for a high-gradient, pool-riffle stream, *Physical Geography* **17**: 142-
742 156.

743 Thompson DM. 2006. The role of vortex shedding in the scour of pools. *Advances in*
744 *Water Resources* **29**: 121-129. DOI:10.1016/j.advwatres.2005.03.015.

745 Thornbury WD. 1954. *Principles Of Geomorphology*. John Wiley: New York, NY.

746 Wald A, Wolfowitz J. 1940. On a test whether two samples are from the same
747 population. *The Annals of Mathematical Statistics* **11**: 147-162.

748 Wheaton JM, Brasington J, Darby SE, Merz J, Pasternack GB, Sear D, Vericat D. 2010.
749 Linking geomorphic changes to salmonid habitat at a scale relevant to fish. *River*
750 *Research and Applications* **26**: 469-486. DOI: 10.1002/rra.1305.

751 Wheaton JM, Fryirs KA, Brierley G, Bangen SG, Bouwes N, O'Brien G. 2015.
752 Geomorphic mapping and taxonomy of fluvial landforms. *Geomorphology* **248**:
753 273-295. DOI: <http://dx.doi.org/10.1016/j.geomorph.2015.07.010>.

754 Wilkinson SN, Keller RJ, Rutherford ID. 2004. Phase-shifts in shear stress as an
755 explanation for the maintenance of pool-riffle sequences. *Earth Surface*
756 *Processes and Landforms* **29**: 737-753.

757 Wyrick JR, Pasternack GB. 2015. Revealing the natural complexity of topographic
758 change processes through repeat surveys and decision-tree classification. *Earth*
759 *Surface Processes and Landforms* **41**: 723-737. DOI: 10.1002/esp.3854.

760 Yumoto M, Ogata T, Matsuoka N, Matsumoto E. 2006. Riverbank freeze-thaw erosion
761 along a small mountain stream, Nikko volcanic area, central Japan. *Permafrost*
762 *and Periglacial Processes* **17**: 325-339. DOI: 10.1002/ppp.569.

763
764

765 Figure Captions

766

767 Figure 1. Flow convergence routing landform classification used in this study.

768 Figure 2. Data processing workflow to obtain all topographic variables used in this
769 study.

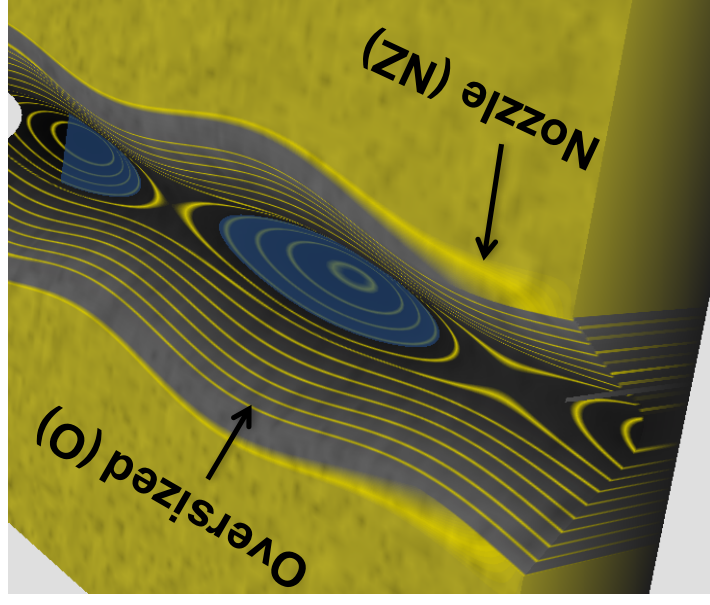
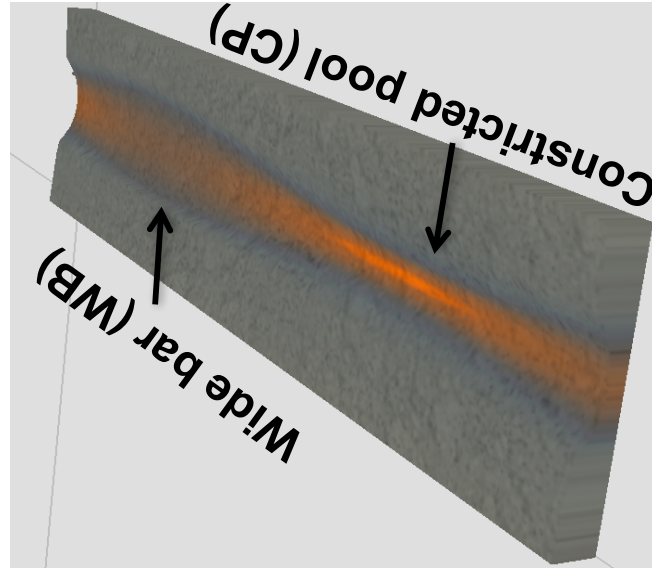
770 Figure 3. Cross-sectional area schematic. Grey denoted the actual wetted cross-
771 section. The black box is the equivalent area as a rectangle given an observed
772 top width. Using thalweg bed elevation (Z_t) would overestimate cross-sectional
773 area, while using the cross-section's average detrended bed elevation (Z_s) would
774 better estimate cross-sectional area.

775 Figure 4. Alternate, interesting flow convergence classifications not used in this study.

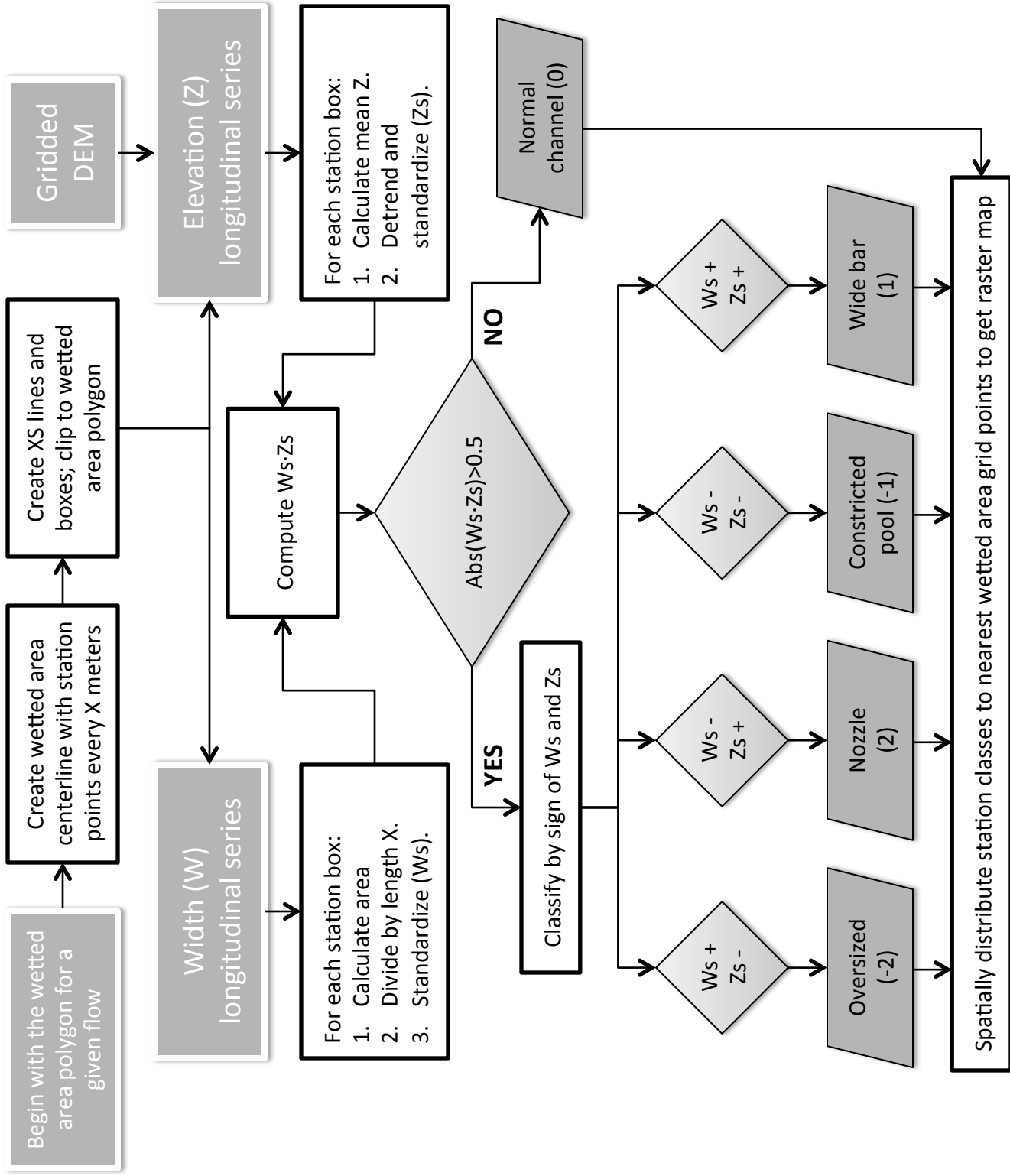
776

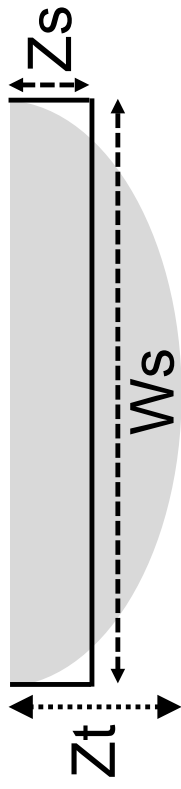
Flow Convergence Routing
Landform Classification*

	Low Ws -	High Ws +
Low Zs -	Constricted pool (CP) -- → +	Oversized (O) -+ → -
High Zs +	Nozzle (NZ) +- → -	Wide bar (WB) ++ → +

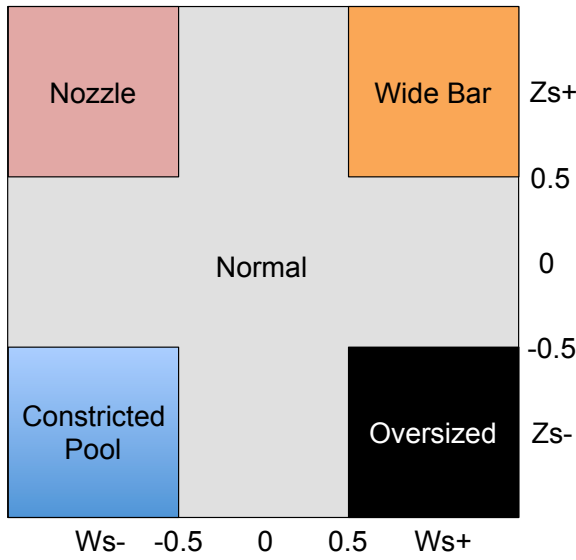


*Ws = standardized width; Zs = detrended, standardized bed elevation





(A) W_s , Z_s extremal classification



(B) W_s , Z_s full classification

